A. Zanoni, M. Zago, R. Paolini, G. Quaranta, M. Galli, P. Masarati
On Task Dependence of Helicopter Pilot Biodynamic Feedthrough and Neuromuscular Admittance: an Experimental and Numerical Study
IEEE Transactions on Human-Machine Systems, In press - Published online 05/01/2021
doi:10.1109/THMS.2020.3044971

On task-dependence of helicopter pilot biodynamic feedthrough and neuromuscular admittance. An experimental and numerical study.

Andrea Zanoni, *Member, IEEE*, Matteo Zago, Rita Paolini, Giuseppe Quaranta, Manuela Galli and Pierangelo Masarati

***Abstract*—The results of a piloted flight simulator campaign aimed at measuring biomechanical performance indicators of a helicopter pilot performing complex, realistic tasks are presented. The upper limbs motion and activation of the main muscle groups of the left arm were measured during ship-deck landings, performed flying several helicopter configurations with sea conditions of variable intensity. The analysis of the results shows an increase in muscle activity relative to the increase in task difficulty, in agreement with subjective ratings (Bedford workload scale). The study provided useful indications to improve the corresponding biomechanical simulations, as well as to characterize pilot performance during specific tasks.**

***Index Terms*—rotorcraft pilot couplings, pilot assisted oscillations, biodynamic feedthrough, pilot workload**

I. Introduction

The action of a helicopter pilot on the aircraft control inceptors (Fig. 1) involves two main contributions: an active one, voluntarily exerted by the pilot in order to control the vehicle, and a passive one, resulting from the involuntary response of the human body to vibrations received from the rotorcraft, primarily through the seat (Fig. 2).

The second contribution is influenced by the first one, as is the case when carrying out tasks that require precision, and/or are to be carried out under intensive workload conditions: the Central Nervous System (CNS) activates the muscles in order to not only provide motion control to the hands and limbs, but also to alter their impedance, by properly modulating the contraction of agonist and antagonist muscles. Generally, when greater precision is required, the CNS activates the involved motor units to increase the equivalent mechanical impedance, an effect that is ordinarily felt as a diffused tension, or stiffening of the affected body parts.

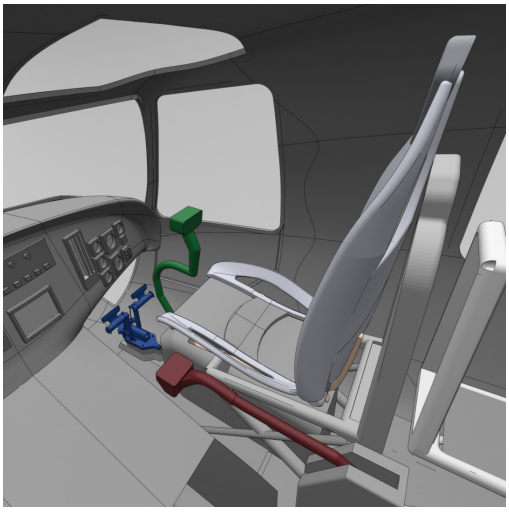

Fig. 1. Schematic view of helicopter control inceptors: the collective inceptor is highlighted in red, the cyclic inceptor in green, and the pedals in blue.

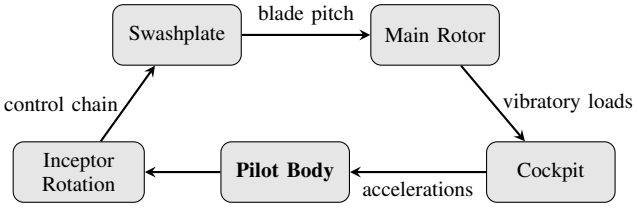

Fig. 2. Rotorcraft-pilot inadvertent coupling through the control system

The passive contribution to the control input can sometimes lead to a degradation of the aircraft handling qualities and, in extreme cases, may result in stability issues that are frequently referred to as Pilot Assisted Oscillations (PAO), a particular kind of Rotorcraft Pilot Couplings (RPC) phenomena [1].
The most common example of RPC is related to the feedback loop of the collective pitch control. The unintentional contribution to the collective pitch input $\Delta\theta_0$ can be further split in two terms: one related to the biomechanical consequence of the cockpit vertical acceleration $\ddot{z}$, when the inceptor is otherwise unloaded, i.e. the Biodynamic Feedthrough (BDFT), and a second one associated with the torque c applied to the inceptor when no vibration affects the cockpit, i.e. the Neuromuscular

Manuscript received Xxxxx XX, 2019; revised Xxxxx XX, 2019.

A. Zanoni is with the Dipartimento di Scienze e Tecnologie Aerospaziali (DAER), Politecnico di Milano, Milan 20156, Italy (e-mail: andrea.zanoni@polimi.it).

M. Zago is with the Dipartimento di Elettronica, Informazione e Bioingegneria (DEIB), Politecnico di Milano, Milan 20133, Italy (e-mail: matteo2.zago@polimi.it).

R. Paolini is with the Dipartimento di Scienze e Tecnologie Aerospaziali (DAER), Politecnico di Milano, Milan 20156, Italy (e-mail: rita.paolini@polimi.it).

G. Quaranta is with the Dipartimento di Scienze e Tecnologie Aerospaziali (DAER), Politecnico di Milano, Milan 20156, Italy (e-mail: giuseppe.quaranta@polimi.it).

M. Galli is with the Dipartimento di Elettronica, Informazione e Bioingegneria (DEIB), Politecnico di Milano, Milan 20133, Italy (e-mail: manuela.galli@polimi.it).

P. Masarati is with the Dipartimento di Scienze e Tecnologie Aerospaziali (DAER), Politecnico di Milano, Milan 20156, Italy (e-mail: pierangelo.masarati@polimi.it).

Admittance (NMA). When the two contributions are expressed through a linearized model of the helicopter's and pilot's small heave perturbations with respect to a reference trim condition, it is possible to write their effect in the Laplace domain as:

$$\Delta\theta_0(s) = H_{\text{BDFT}}(s)\ddot{z}(s) + H_{\text{NMA}}(s)c(s) \tag{1}$$

Clearly, the BDFT depends on the NMA; it actually embeds (and hides) it along with the inceptor dynamics, since equation (1) formally derives from the generalized moment equilibrium of the control inceptor:

$$c(s) = H_{\text{NMA}}^{-1}\left[\Delta\theta_0(s) - H_{\text{BDFT}}(s)\ddot{z}(s)\right] \tag{2}$$

which highlights the fact that the cockpit vibration contribution to the equilibrium of the control inceptor also depends on the neuromuscular admittance.

Understanding – and predicting – the BDFT and NMA is a challenging task, especially when they refer to helicopter control problems. The BDFT and NMA synthesize of the interaction of two complex, non-linear systems: the helicopter and the pilot, both subject to different degrees of variability. The layout of cockpit and inceptors, the inertial parameters of the inceptors and the balancing and trim retaining systems characteristics are among the most important factors that influence the insurgence and danger associated to PAO phenomena. An fundamental role, moreover, is played by the traits of the modes of vibration of the vehicle. The pilot, on the other hand, is also subject to great variability in anthropometric parameters, posture, perceived workload, fatigue, stress, etc., each of which can affect the BDFT and NMA.

This topic has been addressed in the past both experimentally [2] and numerically [3]. BDFT [2], [4], [5] and, to some extent, NMA [6] can be obtained from experimental data in a relatively straightforward manner. However, when doing so, the scope of the information that is conveyed is limited to the specific test environment: the cockpit layout, the mechanical properties of the control inceptors, the anthropometric characteristics [7] and the task [8] the subjects were asked to perform represent factors that can influence both BDFT and NMA. Thoroughly exploring the parameter space may require an enormous amount of effort, time and resources.

Numerical approaches range from low order linear models [9], to detailed, physics based biomechanical models of the human body. Our group has been involved for several years in the development of multibody models of the upper limb and the spine [10], [11], even though the idea is not new: in fact, in 1978 Jex and Magdaleno used a similar, although simplified approach to study vibration feedthrough in semi-supine pilots [3], an unconventional arrangement for which not much experimental data was available at the time. In more recent years, during the project ARISTOTEL [1], a multibody model of the pilot's biomechanics, initially limited to the left arm holding the collective inceptor [10], but later extended to the whole upper body, including the torso, the head, and both arms [11], was developed. The model's parameters can be re-scaled based on height, weight, gender and age of the subject [12].

A. Research goals

The estimation of the dependence of the BDFT from the type of task required workload is still an open area of research [13], especially in relation with helicopter piloting. Research effort in the modeling aspects of the relationship between task, workload and BDFT should follow suit, with the goals of developing design tools that will enhance robustness of novel rotorcraft with respect to RPC/PAO phenomena, analysis tools capable of identifying possible critical issues in current designs, and to exploit a higher-level insight made available from physics-based models into pilot training.

In the context of pilot-in-the-loop helicopter flight simulation of realistic missions, the present research focuses on answering the following questions:

I. is it possible to confirm experimentally the relationship between admittance-control muscle activity and pilot workload?

II. if so, how can the dependence of muscle activation from task workload be introduced in numerical estimation of BDFT and NMA, based on first-principles approaches?

Data about the pose of the pilot's upper limbs and the muscle activity in six left arm muscles were collected during a comprehensive pilot-in-the-loop flight simulator Ship-Helicopter Operational Limitations (SHOL) test campaign, performed on the fixed-base AWARE flight simulation facility at Leonardo Helicopter Division.

The next section briefly outlines the modeling approach followed in the development of multibody biomechanical models of the upper limbs, and the related procedures to extract from simulations the information related to BDFT and NMA. The description of the test campaign and the data analysis conducted to highlight the dependence of the neuromuscular activity from the pilot workload are presented in Section III, and the analysis of collected data can be found in Section IV. Section V describes how the numerical multibody modeling was modified and improved thanks to the lessons learned from the analysis of test data. A recap of the presented work and future developments can be found in Section VI.

II. Multibody Biomechanical Modeling of Pilot Upper Body

The muscles are the actuators of the human body. Typically, multiple bundles produce torque about the same articular joint in agonist/antagonist pairs. Hence, human limbs can be viewed, from the standpoint of their mechanical behavior, as overactuated systems. The result is that multiple activation patterns can yield the same net articular joint torque [14], as shown schematically in Fig. 3. It is evident how the level of *co-contraction*, i.e. of simultaneous contraction of the agonist (in this case, the Biceps Brachii) and of the antagonist (in this case, the Triceps Brachii) in the two depicted cases is different, but the resulting torque about the elbow is the same.

Examining the relationship between the muscle force and the length and contraction velocity of its fibers (Fig. 4), it can be noted how different levels of activation will result in different equivalent muscle impedance about the joint they act upon [15]. The contraction force of a muscle fascicle is, in

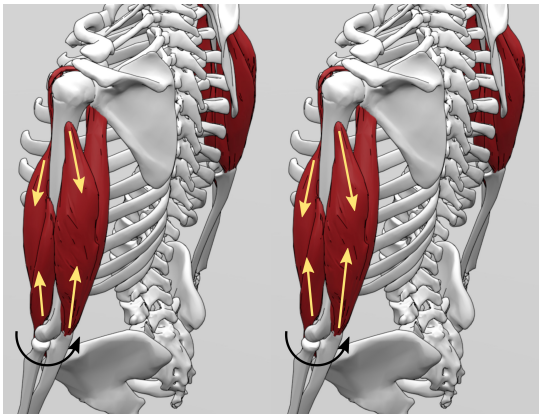

(a) (b)

Fig. 3. Agonist and antagonist muscle bundles: their combined action, with different levels of activation (e.g. (a) and (b)), may generate the same net torque. However, the equivalent impedance may, in general, be different.

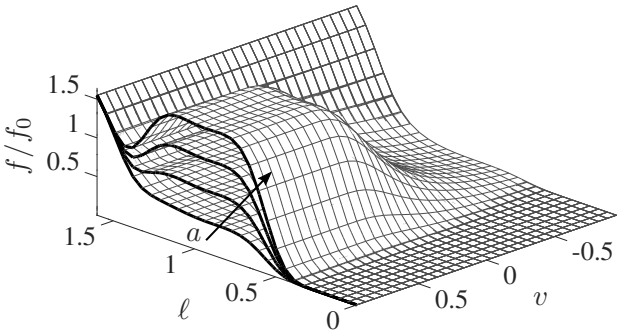

Fig. 4. Muscle non-dimensional isometric contraction force as a function of non-dimensional fiber length and contraction velocity.

fact, a function of the ratio between the actual (ℓ) and the optimal (ℓ_0) fiber length for isometric contraction, $x = \ell/\ell_0$, the ratio between the actual contraction velocity ($\dot{\ell}$) and the optimal one (v_0), $v = -\dot{\ell}/v_0$, and the muscle activation level $a \in [0, 1]$:

$$f = f_0 \left[f_1(\ell) f_2(v) a(t) + f_3(\ell) \right] \tag{3}$$

Helicopter piloting tracking tasks typically involve short and precise movements of the upper limbs and hands, the latter participating with their overall motion in a gripping configuration. Therefore, although in BDFT analysis the dynamics of the torso may play a non-negligible role, in quasi-static analysis detailed multibody modeling can be restricted to the upper limbs: each limb composed of the bony structures related to the scapula, the clavicle, the humerus, the ulna, the radius, and the hand considered as a single rigid body, disregarding the detailed modeling of the fingers. Nodes associated with the bones are connected by ideal kinematic constraints representing the Sternoclavicular (spherical hinge), Acromioclavicular (spherical hinge), Glenohumeral (spherical hinge), Humeroulnar (revolute hinge), Humeroradial (spherical hinge), Radioulnar (point-on-line) and Radiocarpal (Cardano hinge) articular joints. The scapulothoracic joint is modeled as deformable constraint, following the approach outlined in [16]. When the scapular elevation is limited during the simulated task, the motion of the shoulder girdle can be rigidly constrained to that of the torso, and the detailed modeling of the shoulder complex can be disregarded as well, greatly simplifying the model structure [17]. Twenty-five muscles actuate the degrees of freedom of each limb that remain after the application of the kinematic constraints: the humerus adduction-abduction, medio-lateral rotation and flexion-extension, elbow flexion-extension, the forearm prono-supination and the wrist flexion-extension and medio-lateral rotation. The simplified Hill-type muscle actuator model presented in [18] is implemented as the activation-dependent constitutive law of linear viscoelastic actuator elements (rods). Even when the hand is considered as a single rigid body and its trajectory is fully prescribed in terms of both position and orientation, the upper limb is a kinematically underdetermined system: the elbow elevation represents a redundant degree of freedom and, in general, multiple arm configurations can lead to the same hand trajectory. The problem is addressed directly at the position level solving a static problem at each time step, restraining the upper limb nodes through a set of "ergonomy" elastic elements [19], [10], [20]: joint motions associated with stiffer ergonomy springs are thus penalized. The constitutive laws of the ergonomy springs are nonlinear and tailored to comply with the articular joints' limits. Velocity and acceleration problems are then solved in a cascaded-style strategy, based on finite-differences estimations [10], [20].

The joint torques required to yield the estimated kinematics can be easily determined, since the problem is fully determined at this stage. Muscle forces then result from the solution of a constrained minimization problem in the form:

$$\min J(\mathbf{a_0}) = \frac{1}{2}\mathbf{a}_0^T \mathbf{W} \mathbf{a}_0 \qquad \text{s.t.} \tag{4a}$$

$$\mathbf{c} = (\boldsymbol{\theta}^+_{/\mathbf{x}})^T \mathbf{B} \left[\mathbf{F}_a(\mathbf{x}, \dot{\mathbf{x}}) \mathbf{a}_0 + \mathbf{F}_p(\mathbf{x}) \right] \tag{4b}$$

$$0 \leq a_{0i} \leq 1 \tag{4c}$$

In this case, the solution is given by the activation pattern $\mathbf{a}_0$ that minimizes its norm at each time step, subjected to the constraint of producing the joint torques $\mathbf{c}$ while complying with the non-negativity and saturation bounds. Matrix $(\boldsymbol{\theta}^+_{/\mathbf{x}})^T$ represents the pseudo-inverse of the Jacobian matrix of the joint coordinates $\boldsymbol{\theta}$ with respect to the generalized coordinates $\mathbf{x}$, $\mathbf{B}$ is the matrix of (generalized) moment arm of muscle forces with respect to nodal coordinates. Matrix $\mathbf{F}_p$ contains the passive muscle forces, due primarily to tendon elastic elements, and matrix $\mathbf{F}_a$ contains the maximum active muscle forces expressed in the global reference frame, non-linearly depending on the muscle configuration as expressed by equation (3). The resulting activations represent the *minimum effort* activation levels necessary to perform the simulated task. In view of the previously discussed aspects of co-contraction, illustrated in Fig. 3, $\mathbf{a}_0$ can be augmented by an arbitrary perturbation that does not produce a variation in the joint torques $\mathbf{c}$, provided the resulting total activation does not violate the bounds of saturation and non-negativity. Such additional patterns, the *Torque-Less Activation Modes* (TLAMs)

can be found through a decomposition of the incidence matrix $\mathbf{A} = (\boldsymbol{\theta}_{\mathbf{x}}^{+})^{T}\mathbf{B}$ and isolating the singular vectors that are associated with null variation of joint torques.

The neuromuscular admittance in postural control can be divided in two contributions: one depending on the CNS (voluntary) action [21], and the other one, often referred to as *short-range* stiffness [22] independent of the action of the CNS, but rather depending on the intrinsic mechanical characteristics of the muscle tissue [23]. The first effect is sometimes termed *reflexive* contribution to the muscle activation. In the multibody model used in this analysis, this contribution is introduced considering a quasi-steady approximation of the activation dynamics, adding a contribution of the activation proportional to the change in non-dimensional length and normalized contraction velocity of the muscle actuator, through proportional and derivative gains $k_{p,i}$, $k_{d,i}$:

$$a_{r,i} = k_{p,i}\left(\frac{x_i}{x_{i,0}} - \frac{x_{1,\mathrm{ref}}}{x_{i,0}}\right) + k_{d,i}\left(\frac{\dot{x}_i}{v_{i,0}}\right) \tag{5}$$

Currently, the effect of short-range stiffness is not explicitly considered. At least part of its effect can be captured by the quasi-steady model for the reflexive contribution to the total activation, since it is introduced as a function of the perturbation in length and contraction velocity; also the activation dynamics is disregarded. The introduction of the effects of short-range constitutes one of the open points of further model development.

The total activation of the generic muscle actuator is:

$$\mathbf{a} = \mathbf{a}_0 + \mathbf{a}_{\mathrm{TLAM}} + \mathbf{a}_r = \mathbf{a}_0 + \mathbf{K}_{\mathrm{TLAM}}(t)\mathbf{V}_{\mathrm{TLAM}}\mathbf{b} + \mathbf{a}_r \tag{6}$$

where $\mathbf{a}_0$ represents the *baseline* activation, $\mathbf{a}_{\mathrm{TLAM}}$ the contribution due to TLAMs, and $\mathbf{a}_r$ the reflexive contribution. The TLAMs contribution is added as the linear combination of Torque-Less modes, described by the coefficients b and scaled by the time-dependent gains $\mathbf{K}_{\mathrm{TLAM}}(t)$.

III. Experimental Set-up

The relationship between the neuromuscular impedance control performed by the CNS through the modulation of muscle activation, and the amount of effort (physical and mental) the task is requiring has been confirmed in a recent experimental campaign conducted by the authors with a team at Leonardo Helicopter Division [24], [25].

The selected mission was approach and landing of a medium weight helicopter on the flight deck of a frigate-class ship. It is subdivided in the Mission Task Elements (MTEs) depicted in Fig. 5: the approach starts at an altitude of $400\,\mathrm{ft}$ above sea level and $50\,\mathrm{kn}$ forward ground speed (GS); the pilot maneuvers to descend to $50\,\mathrm{ft}$ and reduces the GS to match the ship's speed, to reach a Landing Decision Point (LDP); from the LDP, the pilot was asked to begin a hovering maneuver to wait for a quiescence period in the ship movement, either directly above the landing deck (straight-in approach) or alongside the ship; when the quiescence period was reached, the pilot could initiate the final touch down maneuver. The latter MTE involves high-precision collective control by the pilot, an aspect that contributed to the selection of this kind of mission set-up. Furthermore, the pilot workload is easily modulated, acting on four main parameters:

1) the ship attitude motion, induced by varying the sea state between 0 (calm) to 5 (rough) on the Douglas scale [26];
2) the ship forward motion: it was kept at $0\,\mathrm{kn}$ for all the tests except some of those at sea state 5, in which it was set to $12\,\mathrm{kn}$;
3) the helicopter type and mass configuration: the latter varied between the reference one and maximum take-off weight, maximum aft location of the center of mass;
4) the type of approach the pilot was asked to perform.

When the center of mass is moved aft, the resulting pitch-up attitude of the aircraft reduces visibility and limits collective and cyclic control excursion, increasing the pilot workload. The ship heading has been kept straight into the wind for all tests analyzed in this paper. In most of the test, the ship's attitude was generated by a superposition of harmonic signals, each having random phase. In several test, however, time series recorded in actual sea trials, with sea state 5 and forward velocity $12\,\mathrm{kn}$ were used. The simulated scenario was not meant to be fully representative: for example, the ship's airwake was not taken into account.

The pilot evaluated the subjective workload of each trial immediately after completing the mission. Evaluations were made according to both the Bedford workload ratings [27] and the more specific Deck Interface Pilot Effort Scale (DIPES, Ref. [28]). After some familiarization flights, in which the ship was kept either still or in uniform forward course, without any angular motion, tests were performed with three repetitions for each data point (trial), for a total of 44 runs.

A. Measurement systems and data acquisition

The measurement system used for the tests comprised a motion capture system capable of recording the motion of the pilot's upper body (upper limbs and shoulders) and the electromyography (muscle electrical activity, EMG) of six muscles in the pilot's left arm. The data acquisition system was set up to acquire the signals of the EMG sensors and of the motion capture system in a synchronized fashion using a trigger signal.

a) Motion Capture System: Nine passive markers (diameter: $15\,\mathrm{mm}$) were placed on the sternum, left and right acromia, left humerus medial epicondyle, left and right olecrana, left and right ulna styloid process and right radius styloid process (Fig. 6). Three additional markers were positioned on the collective inceptor. Their 3D trajectories were recorded by eight Near Infra-Red (NIR) cameras (Smart-D, BTS Bioengineering, Milan, Italy) with a sampling rate of $100\,\mathrm{Hz}$.

b) Electromyography: Six wireless probes (Freemg 1000, BTS Bioengineering, Milano, Italy) were placed on the pilot's left *Posterior Deltoid*, *Anterior Deltoid*, *Triceps Brachii*, *Biceps Brachii*, *Extensor Carpi Radialis* and *Flexor Carpi Ulnaris*. Silver-silver chloride bipolar electrodes were placed over the muscle bellies and aligned with expected muscle fiber orientation with a 2-cm inter-electrode distance. The transducers surface electrodes measured the EMG signals of the electrical activity of each muscle group, at a sampling

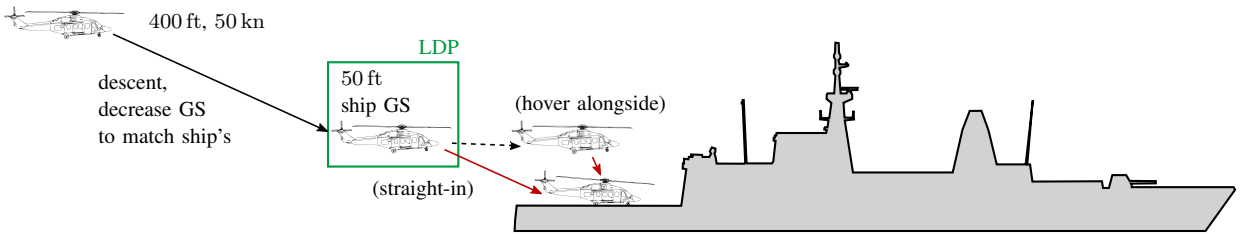

Fig. 5. Mission Task Elements of the ship landing maneuver performed during the flight simulator tests. After the initial descent from 400 ft to 50 ft and the decrease of forward ground speed from 50 kn to match the ship speed the pilot reached the Landing Decision Point (LDP). It was then asked to either hover alongside the ship or to directly move towards the landing deck, wait for quiescence, and touch down.

Fig. 6. Reflective markers and EMG electrodes on the pilot upper body.

frequency of 1000 Hz.
Data concerning the helicopter and ship dynamics and operating conditions were stored by the simulator logging system, with a sampling frequency of 50 Hz. The collective inceptor rotation time history recorded by the stereophotogrammetric motion capture system was used to align the time series of the simulator data, through standard cross-correlation analysis.

IV. Data Analysis

The analysis of the collected signals' time series focused on answering the first research question:

I. is it possible to confirm experimentally the relationship between admittance-control muscle activity and pilot workload?

EMG time series were processed following standard best-practice guidelines [29], [30], [31]. Specifically, they were (i) rectified, (ii) band-pass filtered with 4th-order Butterworth filters, retaining contributions between 1 Hz–20 Hz and (iii) normalized on the peak muscle activation measured in maximum voluntary contractions (MVC) performed prior to the simulated mission under the supervision of a professional physiotherapist.
Data analysis focused on the last 90 s before landing time, i.e. the time instant in which all the weight-on-wheel signals were positive and did not change state any further.

A. Qualitative data analysis

Visual inspection of the time histories related to the helicopter approach to the ship landing spot (LS), compared to the time histories of the EMG activity of the pilot left arm muscles, revealed interesting patterns, illustrated in Figs. 7 and 8. In Fig. 7, representative results obtained for relatively low-workload runs are shown, taking as example a trial in which the vessel had null forward speed, in sea state 3 and the wind speed was 15 kn (Beaufort force 4). The results of a relatively high-workload trial are instead collected in Fig. 8. In this case, the test conditions were far more challenging: the ship was in motion at 12 kn forward speed, the sea state was 5 and the wind speed 25 kn (Beaufort force 6).

Several common traits can be observed in the EMG signals. The muscle activity was concentrated mainly in the forearm muscles, while arm and shoulder muscles show normalized EMG values consistently under 5 % of MVC, thus very small. Furthermore, the EMG activity consistently increased as the distance from the landing spot decreased and the pilot approached the most critical and challenging MTEs. The increase is particularly evident in forearm muscles, since they show a higher average EMG activity level, but it can be noted also in the other muscles. It affects the agonist and the antagonist muscles in the same fashion, indicating that increased *co-contraction* levels are reached in the most challenging phases of the mission. This is an expected result that confirms, qualitatively, that the response of the CNS to increased request for precision in performing a task results in a control of the impedance, obtained increasing the average level of muscle activation of agonist/antagonist pairs.

The concentration of the EMG activity in the forearm was probably due to the high level of experience of the test pilot involved in the experimental study, who extensively developed his technique as a test pilot for the Italian Navy: high precision movement of the collective lever is achieved through a careful control of the forearm and hand muscles, closer to the hand that operates the lever grip, rather than an activity of the upper part of the limb.

B. Quantitative data analysis

A preliminary analysis has been carried out to evaluate the correlation between the Bedford and DIPES ratings given by the pilot to each test point. The results showed a very large correlation (Pearson's coefficient $r > 0.85$) not surprisingly, since the tested scenario involved a very limited set of MTEs upon which the pilot used to judge the required workload. Only the Bedford rating was therefore used to evaluate the correlation with EMG signals.

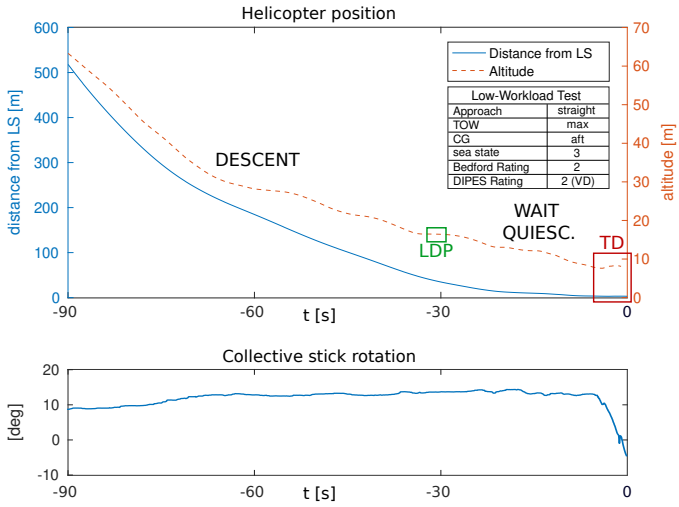

(a) Helicopter data.

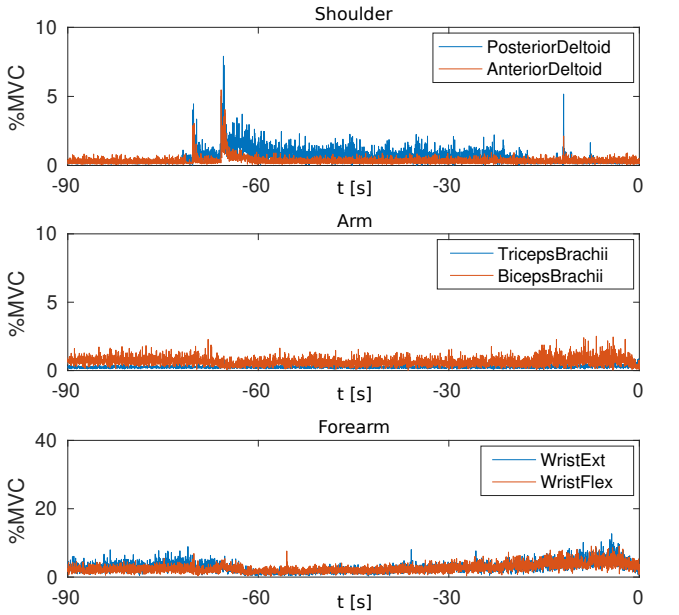

(b) Muscular EMG signals.

Fig. 7. Example results of a low-workload trial (test 33, Cf Tab. II, Appendix B). Helicopter distance from the landing spot, altitude and collective lever rotation are shown in (a). Muscular activities are shown in (b). (TOW: Take-Off Weight; CG: Center of Gravity.)

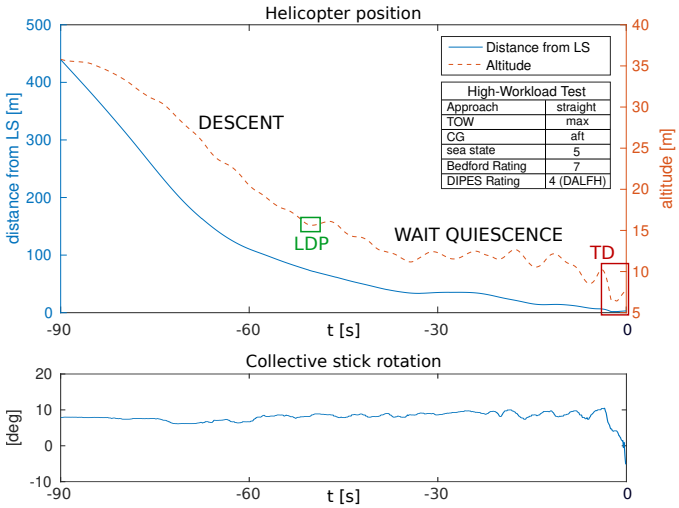

(a) Helicopter data.

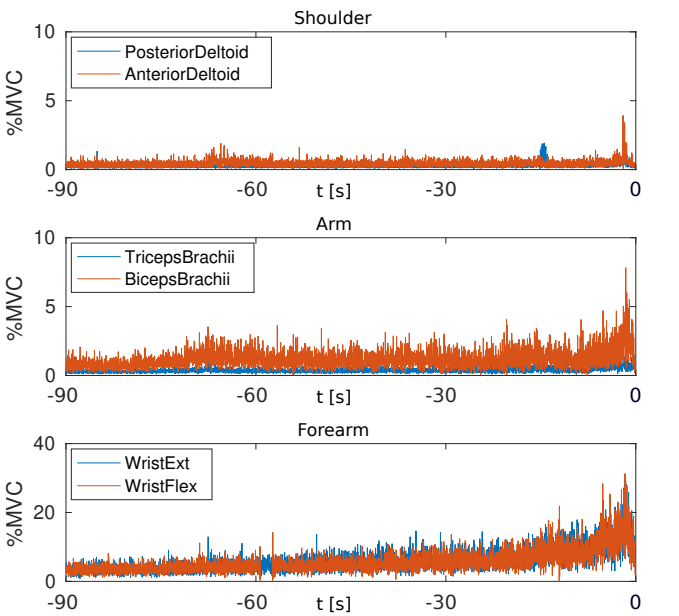

(b) Muscular EMG signals.

Fig. 8. Example results of a high-workload trial (test 29, Cf. Tab. II, Appendix B). Helicopter distance from the landing spot, altitude and collective lever rotation are shown in (a). Muscle activities, expressed in percentage of the Maximum Voluntary Contraction (MVC) are shown in (b).

The Statistical Parameter Mapping (SPM) approach [32], [33], [34], has been used to obtain a time-dependent measure of the signals correlations. Values of the scalar statistics SPM$\{t\}$ outside the selected t-test thresholds are associated with experimental observations in which the correlation between the variability of the outputs (the Bedford rating) and that of the factors (the EMG activities) is statistically significant. Supra or under threshold clusters indicate the time location of positive or negative correlations, assessed through the Spearman correlation coefficient. A significance level of $p = 0.05$ was set. Results of the SPM analysis of EMG signals against Bedford rating signals are shown in Fig. 9. The Biceps Brachii (arm flexor) and the Flexor Carpi Ulnaris (forearm flexor) muscle bundles showed statistical meaningful positive correlation with the Bedford rating in the instants preceding touchdown on the landing deck, which are generally associated with the highest mean EMG activity throughout. It is also noteworthy that the Triceps Brachii (arm extensor) SPM$\{t\}$ value is very close to the selected significance threshold for *positive* correlation in the same time window.

V. Numerical Modeling

The major common trends observed in the experimental results can be summarized in the following:

1) higher relative EMG activity of the forearm muscles, with respect to arm and shoulder muscles;
2) increased EMG activity, especially co-contraction, during the latest portions of the mission, when the helicopter is closer to the landing deck;

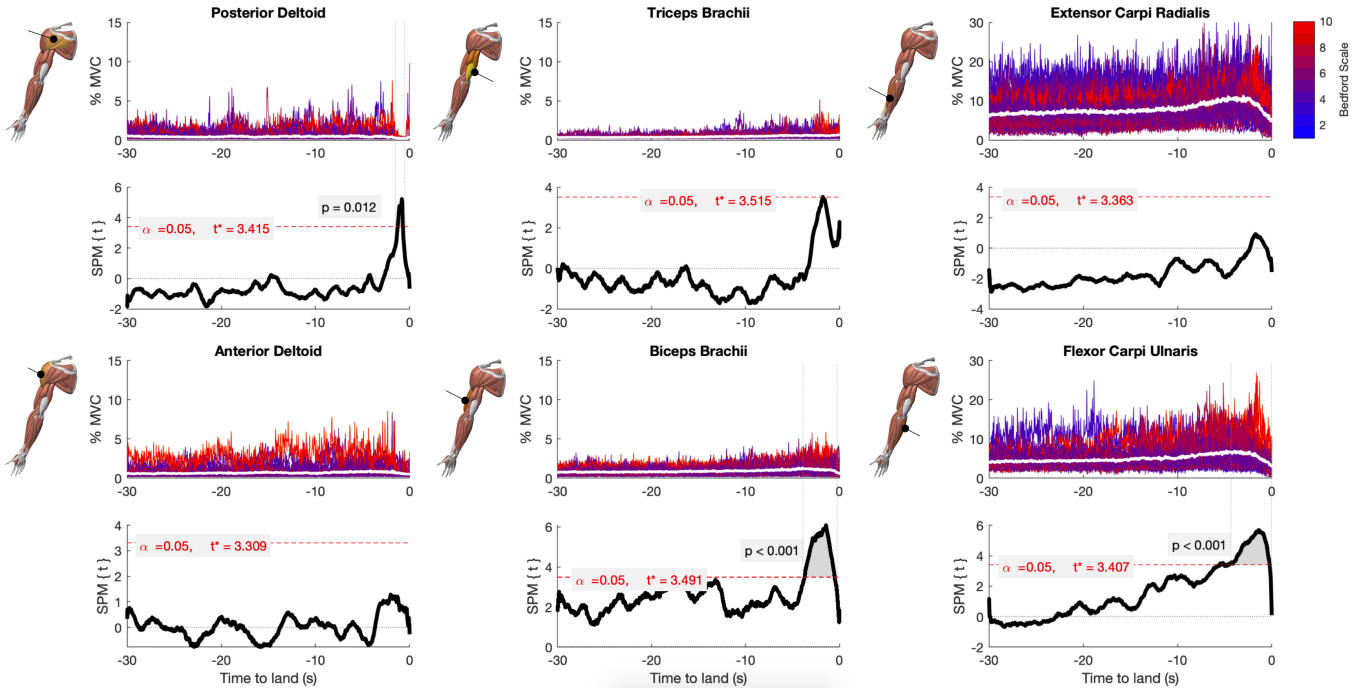

Fig. 9. Activation of agonist/antagonist upper limb muscles in the 30 s preceding landing. Electromyographic (EMG) signals are displayed relative to the Maximum Voluntary Contraction (MVC) and drawn according to the Bedford score reported by the pilot for the corresponding test (see top-right corner; colors shift from blue to red as the score increases). Statistical Parametric Mapping (SPM) plots display the level of significance of the correlation between the reported Bedford Scale score (associated to the whole curve) and the measured EMG value and at each time node. When the SPM(t) value exceeds the statistical threshold, significant correlation clusters were identified (dashed grey lines).

3) across trials, a strong indication of a positive correlation between task workload and muscle activation is found in the latest portion of the mission.

A two-fold approach has been followed in order to enhance the numerical multibody modeling of the pilot biomechanical behavior: some general modifications were introduced to better reproduce the experimental findings regarding the activation strategy; other more specific modifications were then introduced specifically towards modeling task-dependence of muscle activations.

A. Modeling muscle activation strategy

The original cost function used in the computation of the baseline activation, eq. (4a), has been modified introducing the peak isometric muscle force as the weighting factor, in order to favor the activation of the smaller muscles that are found in the forearm. To discourage excessive activation of single muscle bundles, a quartic term has also been added to the resulting cost function:

$$J(\mathbf{a}_0) = \frac{1}{4}\mathbf{a}_0^T \left(\mathbf{a}_0^T \mathbf{F}_0 \mathbf{a}_0\right) \mathbf{a}_0 + \frac{1}{2}\mathbf{a}_0^T \mathbf{F}_0 \mathbf{a}_0 \qquad (7)$$

Since the total activation, as shown by eq. (6), is composed by the sum of the baseline, reflexive and TLAMs activation, also the reflexive activations gains $k_{p,i}$ and $k_{d,i}$ distribution has been modified to favor the contribution of forearm muscles to posture control. A contribution proportional to the inverse of the peak isometric force has been added to the related reflexive activation gains, resulting in the distribution shown in Fig. 10.

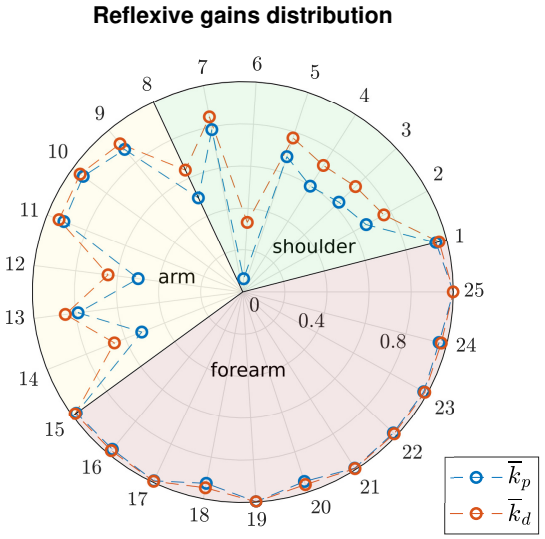

Fig. 10. Distribution of the proportional gain k_p and the derivative gain k_d of the reflexive contribution to the muscle activation, when they are scaled proportionally to the inverse of the maximum isometric contraction force F_0. The circumferential numbers 1–25 refer to the corresponding muscle, according to Table I in Appendix A.

B. Modeling task dependence

The affirmative answer to research question I leads to question II: how can the dependence on muscle activation from task workload be introduced in numerical modeling? Two kinds of approaches can be adopted: *a-posteriori* methods, which rely on the analysis of time series, typically related

to control inputs, to try to determine the pilot instantaneous workload; and *a-priori* methods, that instead try to infer a plausible piloting strategy, and the associated workload factors, from the MTEs features. An example of the first kind is found in the definition of the pilot aggression criterion presented in [35]. The applications of τ-theory to aircraft control, initially proposed by Gareth Padfield and his research group at Liverpool University [36], is instead an example of predictive approach. The basic concept of time-to-target theories has been initially developed in the context of perceptual sciences by Lee [37] and can be synthesized in the assumption that sensory guidance always involves some kind of *gap closure* that the motor control system performs by adapting the closure time $\tau = x/\dot{x}$. Here x takes the role of the relevant gap distance applicable to the task. Pilots' motor control, in the assumptions of τ-theory, builds an instinctive, or *intrinsic* guidance to couple with during task execution.

In the case of SHOL, in the descent and approach phase, the intrinsic guide can be a constant deceleration guide: in [36], the simple cross-over pilot model originally proposed by Kendral and McRuer [38] is modified introducing the τ-coupling behavior, yielding an inverse power law time-dependence of the pilot gain. The same time dependence has been used to drive the gain scheduling of the TLAMs contribution to the total activation, $\mathbf{K}(t)$ of eq. (6). To prevent the gains from reaching values that can lead to activation saturation, and to better fit with experimental observation, a second (negative) inverse power law has been added, to yield

$$K(\hat{t}) = \tilde{k}_1 \left(a - \hat{t}\right)^{-1} + \tilde{k}_2 \left(b - \hat{t}\right)^{-1} \tag{8}$$

where T is the time of task completion, and $\hat{t}$ represents the non-dimensional time to task completion $\hat{t} = t/T$. The parameters a and b, $\tilde{k}_1$ and $\tilde{k}_2$ are adjusted in order to place the curve intersection with the abscissa at $\hat{t} = 1$, and to modulate the maximum gain in relation to the task workload (Fig. 11).

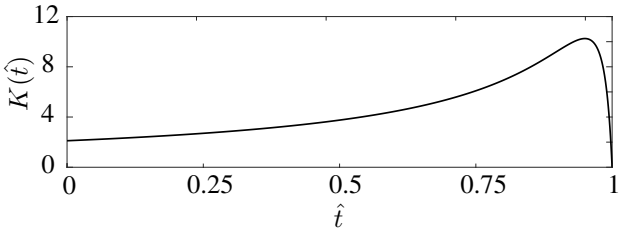

Fig. 11. Gain scheduling of the TLAMs contribution to the overall muscle activation, as a function of the non-dimensional time to task completion.

As evidenced in Fig. 12, the combined effect of the interventions listed above has lead to promising enhancements in matching simulation results to experimental measurements. The muscle activation waveforms were obtained reproducing the experimental tests in numerical simulations, imposing the measured position of the markers to *static* nodes (i.e. having no associated inertial properties) of the upper limbs multibody model, connected to regular nodes through *dummy* springs, analogous to the ergonomy springs used to solve the underdetermined inverse kinematics problem. The initial relative positions of the static nodes with respect to bony segments is estimated; during the simulation, the prestrain $\boldsymbol{\epsilon}$ of the dummy springs is continuously updated. The strain of the elastic element is simply defined as the relative position of the marker with respect to the bony segment node. Therefore, the update scheme is

$$\boldsymbol{\epsilon}_{k+1} = \alpha \mathbf{K}_m^{-1} \boldsymbol{f} + (1 - \alpha)\boldsymbol{\epsilon}_k \tag{9}$$

where α is a constant, set to 0.5 in most simulations, $\mathbf{K}_m$ the (diagonal) stiffness matrix of the elastic element, and $\boldsymbol{f}$ the element internal force. The updating scheme allows to automatically adjust the position of the markers with respect to bony segments nodes in order to minimize the motion reconstruction error.

C. Biodynamic feedthrough

The collective BDFTs, generated by perturbation analysis of the upper limb multibody model about the reference condition of $50\,\%$ collective input are shown in Fig. 13. The transfer functions refer to the collective lever rotation $\Theta(s)$ response to an airframe vertical acceleration input $\ddot{Z}(s)$. Purple, dash-dot lines refer to the original model output, while red, yellow and blue marked lines refer to the modified one, obtained with different TLAMs contribution gains, referring to different non-dimensional mission times $\hat{t}$. The shape of the curves is evidently modified by the different contributions, that were suggested by the behavior of the pilot that performed the tests. Therefore, it can be inferred that piloting style has an influence on the coupling with the aircraft dynamics also at frequencies that are outside of the band of voluntary pilot action. Furthermore, it can be noted that the effect of the present modifications leads, contrary to what one would probably expect, to a *reduction* of the frequency associated with the biodynamic pole and of the BDFT static gain as the pilot approaches the most critical part of the mission. Conversely, the damping of the biodynamic pole is increased in the same conditions. This aspect can be regarded as surprising, since one would expect the frequency of the biodynamic pole to increase in such situation, also in view of results published in the extensive literature available on analytical models of manual tracking tasks [39], [40]. However, the pilot described that in this part of the mission, in which a hovering manoeuvre in the close proximity of the landing deck is performed, he purposely focus on tracking the horizon, as opposed to try to track the movements of the ship, in order to stabilize the aircraft and avoid Pilot Induced Oscillations (PIO) events. In such case, the tracking input is effectively static. However, in absence of extended tests on a larger pilots' cohort (exhibiting different levels of acquaintance with the task at hand), no definite conclusion can be formed. The observed trend could also be related to the underlying nonlinearities, that cannot be completely discarded to properly investigate RPC phenomena.

VI. Conclusions

An extensive flight simulator test campaign of SHOL operations was carried out, and the EMG activity of six muscles of the left upper limb of a single professional test pilot were recorded, together with the trajectories of markers placed on both upper limbs and shoulders. Results of 44 runs of the

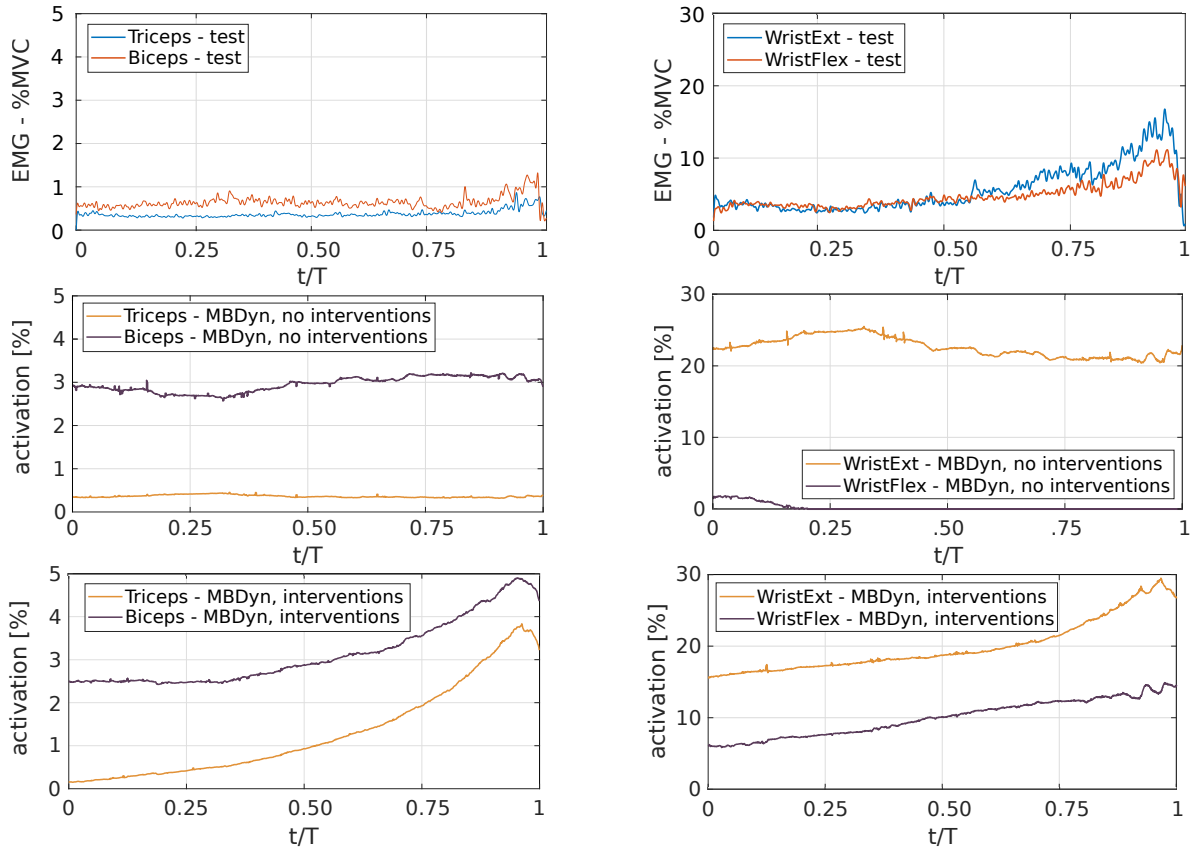

Fig. 12. Comparison between EMG signals time series (top) and computed activation patterns for forearm and arm muscles (mid- and bottom) during a deck landing test. The middle row graphs ('no interventions') show the numerical model results before the described interventions were applied, whereas the last row's ones ('interventions') show results after their application. Signals are referred to the non-dimensional mission time.

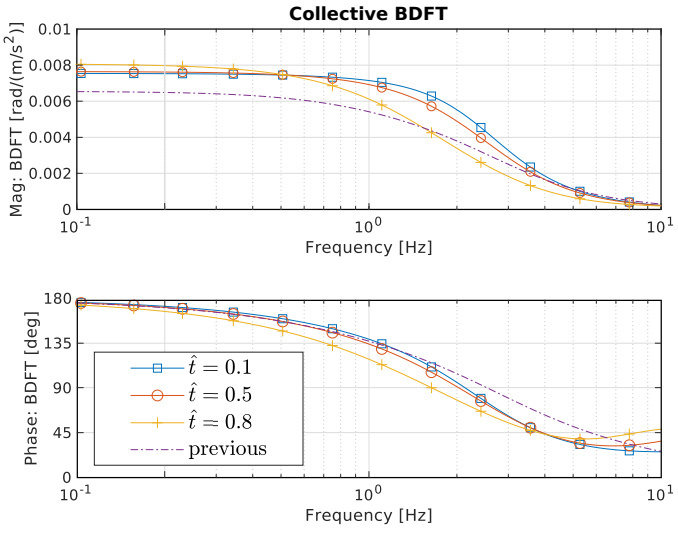

Fig. 13. Numerically estimated collective BDFT functions. The original multibody model output (purple, dash-dot) is compared with the one obtained with the described modifications to baseline activation, reflexive gains and TLAMs gain-scheduling (red, yellow, blue marked lines).

mission task elements under investigation were processed, revealing several common trends: muscle activity tended to be located primarily in the forearm muscles, increasing towards the most challenging portion of the mission, especially in co-contraction configurations; a statistical parameter mapping approach has been used to identify the time-dependent correlation between the muscle activity and the task workload, measured through the Bedford and DIPES ratings given by the pilot at the end of each trial. Results of the SPM showed that indeed a statistical meaningful correlation is present, at least for a subset of the muscle bundles considered, at mission times corresponding to the most challenging MTEs, thus positively answering research question no. I. The experimental results were useful in enhancing the numerical simulations aimed at estimating muscle activity and especially the biodynamic feedthrough of the pilot at the collective control inceptor. An effort to introduce task dependence in numerical simulations has been made, relying on τ-theory to introduce time scheduling of gains regulating the introduction of activation components aimed at modulating the mechanical impedance of the pilot upper limbs, thus positively answering also research question no. II. The results of the numerical simulations showed interesting trends, that are worth of further investigation. The analysis is related to a single pilot and to the collective input; however, care has been given to the search for generality. For example, relying on τ-theory, which results are independent from the specific mission or manoeuvre performed by the pilot; they apply to the individual MTEs in which even complex missions can be split. Furthermore, even if the tests were restricted to the collective input, nothing

specific prevents them to be applicable also to the other channels; in fact, the pilot reported a feeling of tightness also in the right arm and legs muscles in the most challenging segments of the simulated missions.

To better understand the dependence of muscle activity, and thus biodynamic feedthrough, from pilot workload and piloting style, further experimental activities involving multiple pilots with different degrees of experience with respect to the selected mission profiles are envisioned. The tests will be performed on an enhanced testbed, able to directly measure the pilot biodynamic feedthrough, enabling a strong direct validation of the numerical models. Performing the test on a statistically meaningful number of pilots will also be greatly beneficial to the ability of the numerical models to achieve true predictive estimation capability. The analysis of measurements acquired during runs that did not follow the standard maneuver pattern, aimed at highlighting specific phenomena, is also underway at the time of this writing.

ACKNOWLEDGMENTS

This work received partial support from Leonardo Helicopter Division. The authors particularly acknowledge Andrea Ragazzi, Riccardo Bianco Mengotti, and Capt. Andrea Scopa for providing the flight simulator trials and support in collecting the data used in the analysis.

APPENDIX A
MUSCLE ACTUATORS

Naming conventions for muscle actuators in the multibody model are reported in Tab. I. They are used in Fig. 10.

Label	Name	Section
1	Coracobrachialis	Shoulder
2	Anterior Deltoid	Shoulder
3	Medial Deltoid	Shoulder
4	Posterior Deltoid	Shoulder
5	Latissimus Dorsi	Shoulder
6	Pectoralis Major	Shoulder
7	Supraspinatus	Shoulder
8	Infraspinatus	Shoulder
9	Biceps Caput Longus	Arm
10	Biceps Caput Brevis	Arm
11	Anconeus	Arm
12	Triceps Caput Lateralis/Medialis	Arm
13	Triceps Caput Longus	Arm
14	Brachialis	Arm
15	Brachioradialis	Forearm
16	Pronator Teres	Forearm
17	Flexor Carpi Radialis	Forearm
18	Extensor Carpi Ulnaris	Forearm
19	Extensor Digitorum	Forearm
20	Flexor Digitorum Profundus	Forearm
21	Flexor Carpi Radialis	Forearm
22	Extensor Carpi Radialis	Forearm
23	Pronator Quadratus	Forearm
24	Supinator Brevis	Forearm
25	Abductur Pollicis Longus	Forearm

TABLE I
MUSCULAR ACTUATORS IN THE UPPER LIMB MULTIBODY MODEL.

#	Type	Rep.	Heli	W_{TO}	P_{CG}	V_s	Sea	R_{D}	R_{B}
1	A	3	A	STD	STD	0	3	2 HFVD	3
2	A	1	A	STD	STD	0	4	3 HFVD	5
3	A	2	A	STD	STD	0	4	3 HFVD	5
4	A	1	A	STD	STD	0	0	2 Q	2
5	A	2	A	STD	STD	0	0	2 Q	2
6	A	3	A	STD	STD	0	0	2 Q	2
7	A	1	B	STD	STD	0	3	2 LYVD	2
8	A	2	B	STD	STD	0	3	2 LYVD	2
9	A	3	B	STD	STD	0	3	2 LYVD	2
10	A	1	B	STD	STD	0	4	2 LYVD	3
11	A	2	B	STD	STD	0	4	2 LYVD	3
12	A	3	B	STD	STD	0	4	2 LYVD	3
13	A	1	B	STD	STD	0	0	2 LQV	2
14	A	2	B	STD	STD	0	0	2 LQV	2
15	A	3	B	STD	STD	0	0	2 LQV	2
16	A	1	A	STD	STD	0	5	3 VHFD	4
17	A	2	A	STD	STD	0	5	3 VHFD	4
18	A	3	A	STD	STD	0	5	3 VHFD	4
19	S	1	A	STD	STD	12	5	3 VHFD	3
20	S	1	A	MAX	AFT	12	5	4 LD	6
21	S	2	A	MAX	AFT	12	5	4 LD	6
22	A	1	A	MAX	AFT	12	5	4 LD	7
23	A	2	A	MAX	AFT	12	5	4 LD	7
24	A	1	B	MAX	AFT	0	5	5 LFHDAQ	7
25	A	2	B	MAX	AFT	0	5	5 LFHDAQ	7
26	A	3	B	MAX	AFT	0	5	5 LFHDAQ	7
27	S	2	B	MAX	AFT	12	5	3 DALFH	5
28	S	1	B	MAX	AFT	12	5	4 DALFH	7
29	S	2	B	MAX	AFT	12	5	4 DALFH	7
30	A	1	B	MAX	AFT	0	4	3 LQYDV	6
31	A	1	B	MAX	AFT	0	4	4 LQYDV	6
32	A	1	A	MAX	AFT	0	3	2 DV	2
33	A	2	A	MAX	AFT	0	3	2 DV	2
34	A	1	A	MAX	AFT	0	4	3 YHDV	4
35	A	2	A	MAX	AFT	0	4	3 YHDV	4
36	A	3	A	MAX	AFT	0	4	3 YHDV	4
37	A	1	B	MAX	AFT	0	3	3 RYDV	3
38	A	2	B	MAX	AFT	0	3	3 RYDV	3
39	A	3	B	MAX	AFT	0	4	3 RYDV	3
40	A	1	B	MAX	AFT	0	4	3 RYLDV	5
41	A	2	B	MAX	AFT	0	4	3 RYLDV	5
42	A	3	B	MAX	AFT	0	0	3 RYLDV	5
43	A	1	B	MAX	AFT	0	0	2 YLD	3
44	A	2	B	MAX	AFT	0	0	2 YLD	3

TABLE II
PARAMETERS OF THE 44 SIMULATION RUNS.

APPENDIX B
PERFORMED TESTS

Table II collects the parameters for the 44 runs considered in the analysis. The columns contain the following data:

- Type: the type of approach followed after the LDP, either Straight-In (S) or Alongside (A);
- Repetition (Rep.): the test point repetition of the run;
- Heli: the helicopter model employed in the run (A or B);
- W_{TO}: the take-off weight configuration, either standard (STD) or maximum (MAX);
- P_{CG}: the center of mass position, reference (STD) or aft (AFT);
- V_s: the ship's forward velocity;
- Sea: the sea state;
- R_{D}: the pilot's DIPES rating;
- R_{B}: the pilot's Bedford rating.

REFERENCES

[1] M. D. Pavel, M. Jump, B. Dang-Vu, P. Masarati, M. Gennaretti, A. Ionita, L. Zaichik, H. Smaili, G. Quaranta, D. Yilmaz, M. Jones, J. Serafini, and J. Malecki, "Adverse rotorcraft pilot couplings — past, present and future challenges," *Progress in Aerospace Sciences*, vol. 62, pp. 1–51, October 2013, doi:10.1016/j.paerosci.2013.04.003.

[2] J. R. Mayo, "The involuntary participation of a human pilot in a helicopter collective control loop," in *15th European Rotorcraft Forum*, Amsterdam, The Netherlands, 12–15 September 1989, pp. 81.1–12.

[3] H. R. Jex and R. E. Magdaleno, "Biomechanical models for vibration feedthrough to hands and head for a semisupine pilot," *Aviation, Space, and Environmental Medicine*, vol. 49, no. 1–2, pp. 304–316, 1978.

[4] P. Masarati, G. Quaranta, and M. Jump, "Experimental and numerical helicopter pilot characterization for aeroelastic rotorcraft-pilot couplings analysis," *Proc. IMechE, Part G: J. Aerospace Engineering*, vol. 227, no. 1, pp. 124–140, January 2013, doi:10.1177/0954410011427662.

[5] J. Venrooij, D. Yilmaz, M. D. Pavel, G. Quaranta, M. Jump, and M. Mulder, "Measuring biodynamic feedthrough in helicopters," in *37th European Rotorcraft Forum*, Gallarate, Italy, September 13–15 2011, pp. 199.1–12.

[6] J. Venrooij, D. A. Abbink, M. Mulder, M. M. van Paassen, and M. Mulder, "A method to measure the relationship between biodynamic feedthrough and neuromuscular admittance," *IEEE Transactions on Systems, Man, and Cybernetics, Part B: Cybernetics*, vol. 41, no. 4, pp. 1158–1169, 2011, doi:10.1109/TSMCB.2011.2112347.

[7] A. Zanoni and V. Muscarello, "Moving towards a-priori identification of undesirable pilot biometrics for collective bounce instability," in *43rd European Rotorctaft Forum*, Milano, Italy, September 12–15 2017.

[8] J. Venrooij, D. A. Abbink, M. Mulder, M. M. van Paassen, and M. Mulder, "Biodynamic feedthrough is task dependent," in *2010 IEEE International Conference on Systems Man and Cybernetics (SMC)*, Istanbul, Turkey, October 10–13 2010, pp. 2571–2578, doi:10.1109/ICSMC.2010.5641915.

[9] J. Venrooij, M. Mulder, D. Abbink, M. van Paassen, M. Mulder, F. van der Helm, and H. Bulthoff, "Mathematical biodynamic feedthrough model applied to rotorcraft," *Cybernetics, IEEE Transactions on*, vol. 44, no. 7, pp. 1025–1038, July 2014, doi:10.1109/TCYB.2013.2279018.

[10] P. Masarati, G. Quaranta, and A. Zanoni, "Dependence of helicopter pilots' biodynamic feedthrough on upper limbs' muscular activation patterns," *Proc. IMechE Part K: J. Multi-body Dynamics*, vol. 227, no. 4, pp. 344–362, December 2013, doi:10.1177/1464419313490680.

[11] ——, "A detailed biomechanical pilot model for multi-axis involuntary rotorcraft-pilot couplings," in *41st European Rotorcraft Forum*, Munich, Germany, September 1–4 2015.

[12] A. Zanoni and P. Masarati, "Geometry generation and benchmarking of a complete multibody model of the upper limb," in *Fourth Joint International Conference on Multibody System Dynamics - IMSD 2016*, Montréal, Québec, Canada, May 29 - June 2 2016.

[13] J. Venrooij, M. Olivari, and H. H. Bülthoff, "Biodynamic Feedthrough: Current Status and Open Issues," *IFAC-PapersOnLine*, vol. 49, no. 19, pp. 120–125, jan 2016.

[14] R. Enoka, *Neuromechanics of Human Movement-5th Edition*. Human Kinetics, 2015. [Online]. Available: https://books.google.it/books?id=NDDJBgAAQBAJ

[15] N. Hogan, "Adaptive Control of Mechanical Impedance by Coactivation of Antagonist Muscles," *IEEE Transactions on Automatic Control*, vol. 29, no. 8, pp. 681–690, 1984.

[16] B. Bolsterlee, H. E. J. Veeger, and F. C. T. Helm, "Modelling clavicular and scapular kinematics: from measurement to simulation," *Medical & Biological Engineering & Computing*, vol. 52, no. 3, pp. 283–291, 2013. [Online]. Available: http://dx.doi.org/10.1007/s11517-013-1065-2

[17] J. Ambrósio, C. Quental, B. Pilarczyk, J. ao Folgado, and J. Monteiro, "Multibody biomechanical models of the upper limb," *Procedia {IUTAM}*, vol. 2, pp. 4–17, 2011, {IUTAM} Symposium on Human Body Dynamics. [Online]. Available: http://www.sciencedirect.com/science/article/pii/S2210983811000034

[18] E. Pennestrì, R. Stefanelli, P. P. Valentini, and L. Vita, "Virtual musculo-skeletal model for the biomechanical analysis of the upper limb," *Journal of Biomechanics*, vol. 40, no. 6, pp. 1350–1361, 2007, doi:10.1016/j.jbiomech.2006.05.013.

[19] A. Fumagalli, G. Gaias, and P. Masarati, "A simple approach to kinematic inversion of redundant mechanisms," in *ASME IDETC/CIE 2007*, Las Vegas, Nevada, 4–7 September 2007, (DETC2007-35285).

[20] A. Zanoni, A. Cocco, and P. Masarati, "Multibody dynamics analysis of the human upper body for rotorcraft–pilot interaction," *Nonlinear Dynamics*, vol. 102, no. 3, pp. 1517–1539, Nov. 2020. [Online]. Available: https://doi.org/10.1007/s11071-020-06005-7

[21] S. Stroeve, "Impedance characteristics of a neuromusculoskeletal model of the human arm I. posture control," *Biological Cybernetics*, vol. 81, no. 5–6, pp. 475–494, 1999, doi:10.1007/s004220050577.

[22] P. M. H. Rack and D. R. Westbury, "The short range stiffness of active mammalian muscle and its effect on mechanical properties," *The Journal of Physiology*, vol. 240, no. 2, pp. 331–350, jul 1974. [Online]. Available: http://doi.wiley.com/10.1113/jphysiol.1974.sp010613

[23] F. De Groote, J. L. Allen, and L. H. Ting, "Contribution of muscle short-range stiffness to initial changes in joint kinetics and kinematics during perturbations to standing balance: A simulation study," *Journal of Biomechanics*, vol. 55, pp. 71–77, 2017. [Online]. Available: http://dx.doi.org/10.1016/j.jbiomech.2017.02.008

[24] A. Zanoni, M. Zago, R. Paolini, G. Quaranta, P. Masarati, M. Galli, G. Maisano, L. Frigerio, and M. Murawa, "Biodynamic testing for the prediction of rotorcraft-pilot couplings," in *75th Annual Forum of the Vertical Flight Society*, Philadelphia, PA, USA, May 13–16 2019.

[25] ——, "Flight simulator testing to enhance comprehension and modeling of rotorcraft pilot couplings," in *45th European Rotorcraft Forum*, Warsaw, Poland, September 17–20 2019.

[26] N. Bowditch, *American Practical Navigator: an epitome of navigation*. Defense Mapping Agency Hydrographic Center, 1975, vol. 2.

[27] A. Roscoe and G. Ellis, "A subjective rating scale for assessing pilot workload in flight: A decade of practical use," Royal Aerospace Establishment, TR 90019, 1990.

[28] J. S. Forrest, S. J. Hodge, I. Owen, and G. D. Padfield, "Towards fully simulated ship-helicopter operating limits: The importance of ship airwake fidelity," in *AHS 64th Annual Forum*, Montréal, Canada, April 29–May 1 2008.

[29] D. A. Winter, *Biomechanics and Motor Control of Human Movement*, 2nd ed. New York: Wiley, 1990.

[30] M. Cifrek, V. Medved, S. Tonkovič, and S. Ostoijč, "Surface emg based muscle fatigue evaluation in biomechanics," *Clinical Biomechanics*, vol. 24, no. 4, pp. 327–340, 2009.

[31] R. Neptune, I. C. Wright, and A. Van Den Bogert, "Muscle coordination and function during cutting movements," *Medicine Science in Sports and Exercise*, vol. 31, no. 2, pp. 294–302, 1999.

[32] W. D. Penny, K. J. Friston, J. T. Ashburner, S. J. Kiebel, and T. E. Nichols, *Statistical parametric mapping: the analysis of functional brain images*. Elsevier, 2011.

[33] T. C. Pataky, "Generalized n-dimensional biomechanical field analysis using statistical parametric mapping," *Journal of Biomechanics*, vol. 43, no. 10, pp. 1976–1982, 2010. [Online]. Available: http://dx.doi.org/10.1016/j.jbiomech.2010.03.008

[34] T. C. Pataky, J. Vanrenterghem, and M. A. Robinson, "Zero- vs. one-dimensional, parametric vs. non-parametric, and confidence interval vs. hypothesis testing procedures in one-dimensional biomechanical trajectory analysis." *Journal of Biomechanics*, vol. 48, no. 7, pp. 1277 – 1285, 2015.

[35] M. Jones, M. Jump, and L. Lu, "Development of the phase-aggression criterion for rotorcraft pilot couplings," *J. of Guidance, Control, and Dynamics*, vol. 36, no. 1, pp. 35–47, January-February 2013, doi:10.2514/1.58232.

[36] G. Padfield, "The tau of flight control," *The Aeronautical Journal*, vol. 115, pp. 521–555, 09 2011.

[37] D. Lee, "A theory of visual control of braking based on information about time-to-collision," *Perception*, vol. 5, pp. 437–59, 02 1976.

[38] D. T. McRuer and E. S. Krendel, "Mathematical models of human pilot behavior," Systems Technology, Inc., 13766 S. Hawthorne Boulevard Hawthorne, California 90250-7083, Paper No. 146, January 1974, AGARD AG 188.

[39] D. T. McRuer and H. R. Jex, "A review of quasi-linear pilot models," *Human Factors in Electronics, IEEE Transactions on*, vol. HFE-8, no. 3, pp. 231–249, September 1967, doi:10.1109/THFE.1967.234304.

[40] K. van der El, D. M. Pool, M. R. M. van Paassen, and M. Mulder, "Effects of target trajectory bandwidth on manual control behavior in pursuit and preview tracking," *IEEE Transactions on Human-Machine Systems*, vol. 50, no. 1, pp. 68–78, 2020.